

Band evolution of two-dimensional transition metal dichalcogenides under electric fields

Cite as: Appl. Phys. Lett. **115**, 083104 (2019); <https://doi.org/10.1063/1.5093055>

Submitted: 24 February 2019 . Accepted: 27 July 2019 . Published Online: 21 August 2019

Peng Chen, Cai Cheng, Cheng Shen, Jing Zhang, Shuang Wu, Xiaobo Lu, Shuopei Wang, Luojun Du, Kenji Watanabe , Takashi Taniguchi, Jiatao Sun, Rong Yang, Dongxia Shi, Kaihui Liu, Sheng Meng, and Guangyu Zhang 



View Online



Export Citation



CrossMark

ARTICLES YOU MAY BE INTERESTED IN

[Valley dynamics of different trion species in monolayer WSe₂](#)

Applied Physics Letters **115**, 082101 (2019); <https://doi.org/10.1063/1.5112823>

[Design of metal contacts for monolayer Fe₃GeTe₂ based devices](#)

Applied Physics Letters **115**, 083105 (2019); <https://doi.org/10.1063/1.5118304>

[Multifunctional anti-ambipolar p-n junction based on MoTe₂/MoS₂ heterostructure](#)

Applied Physics Letters **115**, 073104 (2019); <https://doi.org/10.1063/1.5109221>

Lock-in Amplifiers
Find out more today



 Zurich Instruments

Band evolution of two-dimensional transition metal dichalcogenides under electric fields

Cite as: Appl. Phys. Lett. **115**, 083104 (2019); doi: [10.1063/1.5093055](https://doi.org/10.1063/1.5093055)

Submitted: 24 February 2019 · Accepted: 27 July 2019 ·

Published Online: 21 August 2019



View Online



Export Citation



CrossMark

Peng Chen,^{1,2,3,4} Cai Cheng,^{1,4} Cheng Shen,^{1,4} Jing Zhang,^{1,4} Shuang Wu,^{1,4} Xiaobo Lu,^{1,4} Shuopei Wang,^{1,4} Luojun Du,^{1,4} Kenji Watanabe,⁵  Takashi Taniguchi,⁵ Jiatao Sun,^{1,4} Rong Yang,^{1,4} Dongxia Shi,^{1,4} Kaihui Liu,⁶ Sheng Meng,^{1,4} and Guangyu Zhang^{1,4,7,8,9,a)} 

AFFILIATIONS

¹Beijing National Laboratory for Condensed Matter Physics and Institute of Physics, Chinese Academy of Sciences, Beijing 100190, China

²State Key Laboratory for Chemo/Biosensing and Chemometrics, College of Chemistry and Chemical Engineering, Hunan University, Changsha 410082, China

³Department of Chemistry and Biochemistry and California Nanosystems Institute, USA; University of California, Los Angeles, California 90095, USA

⁴School of Physical Sciences, University of Chinese Academy of Sciences, Beijing 100190, China

⁵Advanced Materials Laboratory, National Institute for Materials Science, 1-1 Namiki, Tsukuba 305-0044, Japan

⁶State Key Laboratory for Mesoscopic Physics, School of Physics, Peking University, Beijing 100871, China

⁷Collaborative Innovation Center of Quantum Matter, Beijing 100190, China

⁸Beijing Key Laboratory for Nanomaterials and Nanodevices, Beijing 100190, China

⁹Songshan-Lake Materials Laboratory, Dongguan 523808, Guangdong Province, China

a) Author to whom correspondence should be addressed: gyzhang@iphy.ac.cn

ABSTRACT

Band engineering of two-dimensional transition metal dichalcogenides (2D TMDCs) is of great significance with regard to both fundamental exploration and practical application. Here we report on a study of the band evolution of monolayer and bilayer TMDCs (WS_2 , WSe_2 , and MoS_2) under vertical electric fields. Our results show that the electric field has a negligible influence on the bandgaps of monolayer TMDCs. For bilayer TMDCs, our results show that their intralayer direct bandgaps are also immune to the electric field. However, the indirect bandgaps of bilayer TMDCs can be effectively tuned by a vertical electric field. Interestingly, we find that the field tunability of the bandgap in bilayer WSe_2 is much larger than those in bilayer WS_2 and MoS_2 .

Published under license by AIP Publishing. <https://doi.org/10.1063/1.5093055>

Two-dimensional transition metal dichalcogenides (TMDCs) have recently emerged as a new class of semiconductor materials and have attracted a considerable amount of attention.^{1–16} Such atomically thin materials show promise for use in the next generation of electronic and optoelectronic devices such as logic modules, light-emitting diodes, lasers, and photodetectors. To fully explore this potential, a prerequisite is the ability to engineer the band structures of these materials. In contrast to conventional semiconductors, using an external electric field is an effective and flexible approach to tune the band structure of 2D TMDCs owing to their ultrathin nature.^{17–22} It is known that monolayer TMDCs are direct bandgap semiconductors and bilayer TMDCs are indirect bandgap semiconductors.¹ However,

previous studies of bilayer MoS_2 have not shown any indirect bandgap evolution under an electric field, which resulted from the inferior photoluminescence (PL) quality in their devices due to inhomogeneous line broadening.²⁰ The PL of 2D TMDCs can usually be easily degraded by the impurities and atomic defects that are introduced during the device fabrication process.

To shed light on the issue of band evolution, we utilize the van der Waals integration technique to construct devices, enabling us to study the intrinsic properties of 2D TMDCs under an electric field. Our PL measurements show that the electric field has a negligible influence on the bandgaps of monolayer TMDCs. For bilayer TMDCs, the intralayer direct band transition is also immune to the electric field.

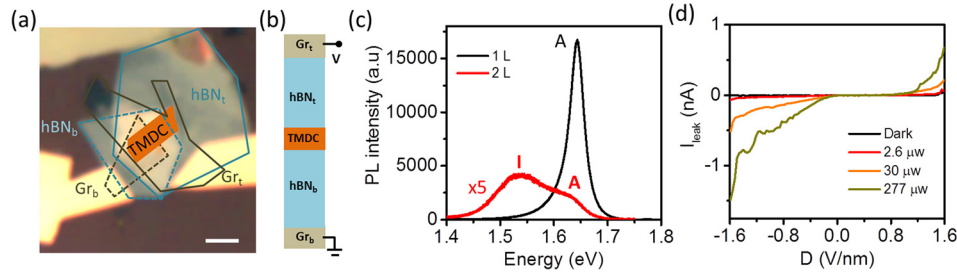


FIG. 1. (a) Optical microscope image of a van der Waals heterostructure device. Scale bar = 5 μm . (b) Schematic diagram of the device. A DC voltage V is applied between the top and bottom graphene electrodes Gr_t and Gr_b . (c) PL spectra of monolayer and bilayer WSe_2 in the van der Waals heterostructure. For the monolayer WSe_2 , the A peak (at ~ 1.64 eV) corresponds to the A exciton; for the bilayer WSe_2 , the A peak (at ~ 1.64 eV) and I peak (at ~ 1.53 eV) correspond to the A exciton and the indirect bandgap transition, respectively. (d) Leakage current–displacement field characteristics of the van der Waals heterostructure device with and without 532 nm laser illumination.

However, the indirect bandgaps of bilayer TMDCs can be effectively tuned by a vertical electric field. These results are consistent with the theoretical calculations. In addition, we find that the field tunability of bandgap in bilayer WSe_2 is much larger than those in bilayer WS_2 and MoS_2 .

Figures 1(a) and 1(b) show the architecture of our devices. We encapsulated a 2D TMDC with hexagonal boron nitride (hBN) to form an hBN/2D TMDC/hBN van der Waals heterostructure (Materials and methods, [supplementary material](#)). The surface of the hBN crystal is atomically smooth and nearly free from charge trapping and dangling bonds, preserving the high quality of the encapsulated 2D crystals.^{23–31} Owing to the high quality of the samples, the 2D TMDCs show well-distinguished PL peaks at room temperature (Fig. S1, [supplementary material](#)). Two transparent graphene electrodes were used to apply a vertical electric field to this sandwich structure. The displacement field D in a 2D TMDC is estimated to be $D = \epsilon_{\text{hBN}} V / (d_1 + d_2)$, where $\epsilon_{\text{hBN}} \sim 3.5$ is the dielectric constant of hBN,³² V is the applied bias voltage, and d_1 and d_2 are the thicknesses of hBN_t and hBN_b , respectively (Materials and methods, [supplementary material](#)). The band structures of the 2D TMDCs are very similar. The monolayer and bilayer TMDCs are direct and indirect bandgap semiconductors, respectively. PL spectroscopy is a powerful tool to study the band structures of 2D TMDCs. For monolayer TMDCs, the PL spectrum is contributed by the direct bandgap transition at the K point (the A exciton). For bilayer TMDCs, the PL spectrum is contributed by the

intralayer direct band transition at the K point (the A exciton) and the indirect band transition between the valence band maximum at the Γ_v point and the conduction band minimum (CBM) at the K point or Λ_c point. The energy of the indirect band transition is lower than that of the direct band transition in bilayer TMDCs. Note that the exact position of the conduction band minimum in different 2D TMDCs is still not clear and is a matter of current debate.^{33–36} Figure 1(c) shows the PL spectrum of monolayer and bilayer WSe_2 in our heterostructure devices. For the monolayer WSe_2 , the A peak (at ~ 1.64 eV) corresponds to the A exciton; for the bilayer WSe_2 , the A peak (at ~ 1.64 eV) and the I peak (at ~ 1.53 eV) correspond to the A exciton and the indirect bandgap transition, respectively. Figure 1(d) shows the leakage current–displacement field characteristic measurements with and without 532 nm laser illumination. To ensure that the applied electric field did not cause breakdown of the devices, the leakage currents were kept below 5 nA in our experiments.

Figures 2(a)–2(c) show the PL spectra of bilayer WSe_2 , WS_2 , and MoS_2 at various vertical displacement fields. The PL spectra of bilayer TMDCs are contributed by both the direct and indirect band transitions, and the bandgaps of few-layer TMDCs can be studied by examining the indirect band transition. Under vertical displacement fields, the energies of indirect band transition in bilayer WSe_2 , WS_2 , and MoS_2 show significant red shifts, indicating reduced bandgaps. The tunable bandgaps of bilayer TMDCs under displacement fields can be understood in terms of the band splitting of monolayers that are

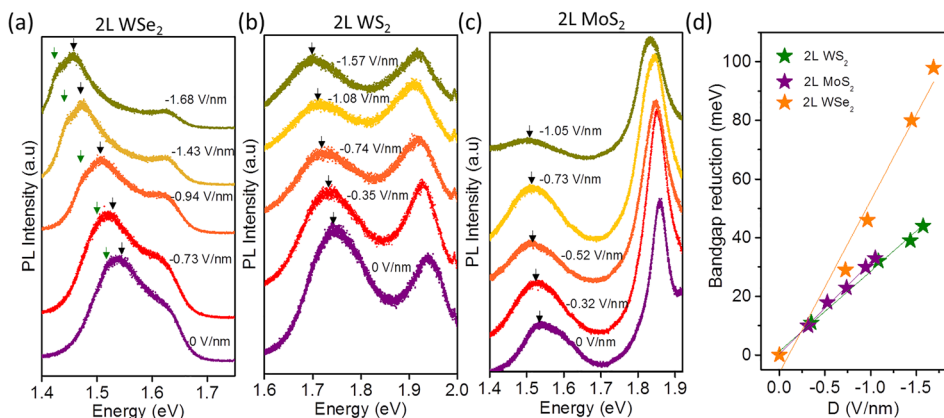


FIG. 2. (a) PL spectra of bilayer WSe_2 under various displacement fields. The indirect band of bilayer WSe_2 split into two peaks, I1 and I2, the positions of which are indicated by the black and green arrows, respectively. (b) PL spectra of bilayer WS_2 under various displacement fields. The black arrows indicate the peak positions of the indirect band transition. (c) PL spectra of bilayer MoS_2 under various displacement fields. The black arrows indicate the peak positions of the indirect band transition. (d) Indirect bandgap reduction of different bilayer TMDCs under various displacement fields. The solid lines are the linear fits to the data points.

weakly coupled via van der Waals interactions. In the absence of an applied displacement field, the energy bands of bilayer TMDCs are contributed equally by the top and bottom layers. However, when subjected to a vertical displacement field, the energy degeneracy of each layer is broken by the electric potential difference between the two monolayers. The energy bands of the top and bottom layers move toward each other, reducing the bandgap. This phenomenon is different from the atomic level Stark effect, and is dubbed the giant Stark effect.¹⁹ The experimental results are very robust and highly repeatable. We investigated four bilayer devices with different hBN thicknesses and found that all these devices show similar field response (Fig. S2, [supplementary material](#)). We note that in these van der Waals heterostructure devices, the 2D TMDCs can be potentially doped by tunneling charges, which may influence the energy of the indirect band transition. To evaluate the influence of charge doping on our experimental results, we performed measurements with a dual-gate geometry in which both the charge doping and displacement fields were controlled by the dual gate. The results show that the energy of the indirect band transition is almost immune to charge doping in our experiments (Fig. S3, [supplementary material](#)).

[Figure 2\(d\)](#) summarizes the field-dependent indirect bandgap reduction in bilayer WSe_2 , WS_2 , and MoS_2 . It can be seen that the field tunability of the bandgap differs significantly among different bilayer TMDCs. From the linear fit of the data points in [Fig. 2\(d\)](#), we obtain the magnitude of the energy shift of the indirect band transition as 59 meV V/nm for 2L WSe_2 , 31 meV V/nm for 2L MoS_2 and 27 meV V/nm for 2L WS_2 . The shift of the indirect bandgap under a displacement field in bilayer WSe_2 is more pronounced than in bilayer MoS_2 and WS_2 . Several reasons could potentially contribute to the differences in field tunability of bilayer WSe_2 , WS_2 , and MoS_2 . Previous theoretical studies have shown that the field tunability of the bandgap scales with the interlayer spacing of a bilayer TMDC. A larger interlayer spacing can lead to increased field tunability.¹⁷ The interlayer spacing of a TMDC is correlated with its chalcogen element, and TMDCs containing heavier chalcogen elements have larger interlayer spacing than those containing lighter chalcogen elements.³⁷ As a result, TMDCs containing a heavier chalcogen element (Se) should have an increased field response. Besides the interlayer spacing, the

different charge transfer abilities of 2D TMDCs containing different chalcogen elements under an electric field might also play an important role. Calculations of charge redistribution of bilayer TMDCs under electric fields suggest that there is a progressive depletion of charge density in the chalcogen p_z orbitals with increasing displacement field.¹⁷ Conversely, there is accumulation of charge density in the transition metal orbitals. The heavier chalcogen atoms have more diffuse p_z orbitals than the lighter chalcogen atoms. As a result, TMDCs with heavier chalcogen atoms can facilitate greater charge transfer from chalcogen atoms to metal atoms in the same displacement field, which may also lead to an increased field response. The effect of switching the transition metal from Mo to W while retaining the chalcogen (S) is not significant, because transition metal atoms have a very small influence on both the interlayer spacing and the charge transfer abilities under electric fields. The initial frontier orbital arrangement may also play an important role in the field response of the bandgap. For example, K valleys are predominantly from transition metal atom d_{xy} , $d_{x^2-y^2}$, and d_{z^2} orbitals, with some chalcogen atom p_x and p_y characters confined within the 2D xy plane, while there is considerable chalcogen atom p_z character at Λ_c and Γ_v .^{17,18,36} These electron orbitals may have different responses to an electric field. Thus, different initial frontier orbital arrangements may lead to considerably different field responses. However, at present, there is still much debate about the frontier orbital arrangements of different TMDCs. We believe that further experimental and theoretical work will be needed to obtain a deeper understanding of why the field response of bilayer WSe_2 can be much larger than that of bilayer WS_2 and MoS_2 .

We next studied the PL spectrum of monolayer TMDCs under displacement fields [[Figs. 3\(a\)](#) and [3\(b\)](#)]. At zero displacement field, the most prominent peak in monolayer WSe_2 is around 1.64 eV, with a relatively weak side-peak around 1.61 eV. These two peaks are classified as neutral exciton (A) and trion (A^-), respectively. With increasing displacement field, the relative weight of the trion increases and its energy shows a red shift, suggesting increased charge doping (Fig. S4, [supplementary material](#)). At high displacement field, the relative weight of the A peak increases again and the energy of the trion shows a blue shift, suggesting decreased charge doping.³⁸ However, the

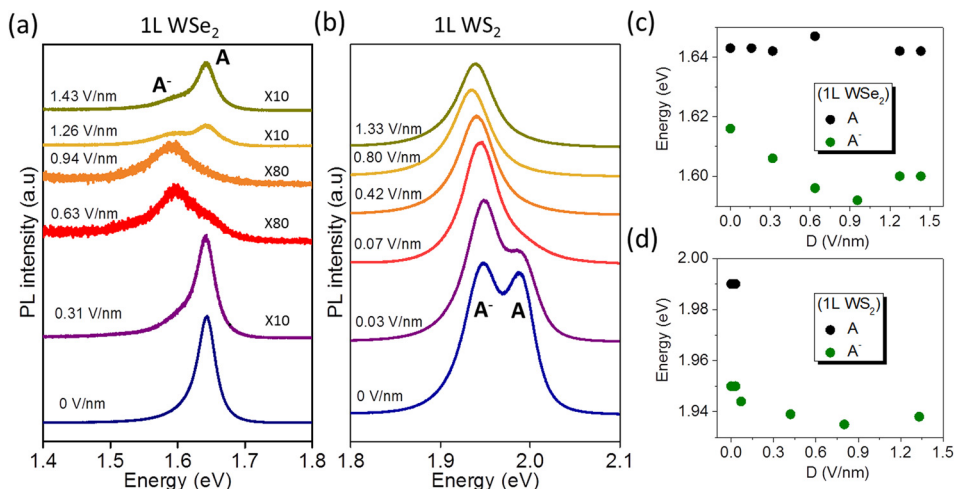


FIG. 3. (a) PL spectra of monolayer WSe_2 under various displacement fields. (b) PL spectra of monolayer WS_2 under different displacement fields. (c) Energies of A and A^- in monolayer WSe_2 under various displacement fields. (d) Energies of A and A^- in monolayer WS_2 under various displacement fields. The black dots indicate the energy of A and the green dots the energy of A^- .

energy of the A peak at $D = 1.4$ V/nm is almost unchanged compared with that at zero displacement field [Fig. 3(c)], indicating that the giant Stark effect is negligible in monolayer TMDCs, which is consistent with previous studies.^{17,20} For monolayer WS_2 , as the field increases, the relative weight of the trion increases and its energy shows a continuous red shift, suggesting increased charge doping [Fig. 3(d)]. However, on further increasing the displacement field to ~ 1.3 V/nm, the energy of the trion shows a blue shift, suggesting that charge doping is decreased in the high-displacement-field regime, which is the same as is observed in monolayer WSe_2 . The charge doping mechanism in the heterostructure device can be understood in terms of a quantum well model.³⁹ In this model, the energy difference between the charge-neutral point of multilayer graphene and the conduction band minimum (CBM) of the TMDC is ~ 0.5 eV. With increasing displacement field, the Fermi level in the bottom graphene electrode (Γ_b) rises above the conduction band minimum of the TMDC, facilitating electron tunneling into the TMDC. On further increasing the displacement field above 1.4 V/nm, the electron doping concentration decreases, because the electrons can be emitted directly from the bottom graphene electrode and collected by the top graphene electrode. This process is consistent with the transport measurements shown in Fig. 1(d), where a rapid photocurrent increase can be observed after $D \geq 1.2$ V/nm.

As the direct peaks of bilayer TMDCs originate from the intralayer transition at the K point, the energy shift of A and A^- in monolayer TMDCs under a displacement field can help in understanding the energy shift of the direct peaks in bilayer TMDCs. As the displacement field increases from zero, the charge doping in bilayer TMDCs increases. Thus, the relative PL emission weight of A^- increases and the energy of A^- shows a continuous red shift. With further increase in the displacement field, charge doping will decrease, and the energy of A^- will show a blue shift. The trion and the neutral exciton are usually not clearly distinguished in few-layer TMDCs. However, we observed an obvious blue shift of the direct peak in bilayer WS_2 at high displacement fields, which unambiguously verified the decreased charge doping in the high-displacement-field regime [Fig. 2(b)].

We performed density functional theory (DFT) calculations to study the influence of electric fields on bilayer TMDCs. As can be seen from Fig. 4(a), the DFT results for bilayer WSe_2 show that an electric field has a strong influence on the indirect bandgap, while the intralayer direct bandgap is almost immune. These DFT results are consistent with our experimental results. Finally, we noticed a splitting of the indirect peak in bilayer WSe_2 [Fig. 2(a)]. This might be attributable to spin splitting of the CBM at the K point in bilayer WSe_2 , since the observed splitting matches well with the DFT value of $\Delta_C \sim 32$ meV. Moreover, Δ_C is independent of the displacement field, which is also consistent with the DFT results [Fig. 4(b)]. The conduction band spin splitting originates from the spin-orbit coupling induced by the chalcogen atom, which is much smaller than the valence band splitting induced by the transition metal.¹ Figures 4(c) and 4(d) show schematic band diagrams of monolayer and bilayer WSe_2 . The VBM at the K point is a spin-up state; the lower (upper) state at CBM is spin-down (up). The VBM at the Γ_v point is a spin-degenerate state. We know that optical transitions occur only between states with the same spin orientation. Thus, we could only observe the transition between the VBM at the K point and the upper state of the CBM at the K point in monolayer WSe_2 . The lower state at CBM is a dark state.⁴⁰ In contrast, for bilayer

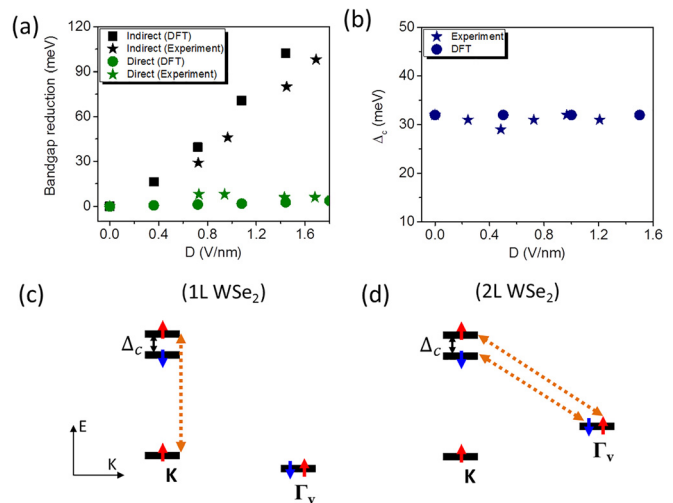


FIG. 4. (a) Displacement field dependence of the bandgap reduction in bilayer WSe_2 . The DFT-calculated and experimental results for indirect bandgap reduction at various displacement fields are denoted by black squares and stars, respectively, and the DFT-calculated and experimental results for intralayer direct bandgap reduction at various displacement fields are denoted by green circles and stars, respectively. (b) Displacement field dependence of indirect band splitting in bilayer WSe_2 . The DFT-calculated and experimental results are denoted by circles and stars, respectively. (c) Band diagram of monolayer WSe_2 . An optical transition can occur between the K point in the valence band and the upper state of the conduction band at the K point. (d) Band diagram of bilayer WSe_2 . An optical transition can occur between the Γ_v point in the valence band and both the upper and lower states of the conduction band at the K point.

WSe_2 , the indirect peak originates from the transition between the CBM at the K point and the VBM at the Γ_v point (a spin-degenerate state). Thus, both the upper and lower states are bright states.

In summary, we have studied the intrinsic band evolution of monolayer and bilayer TMDCs (WS_2 , WSe_2 , and MoS_2) under electric fields using van der Waals heterostructures. Our results show that the electric field has a negligible influence on the bandgaps of monolayer TMDCs. For bilayer TMDCs, our results show that their intralayer direct bandgaps are also immune to the electric field. However, their indirect bandgaps can be effectively tuned by a vertical electric field. Moreover, we have found that the field tunability of the bandgap in bilayer WSe_2 is much larger than those in bilayer WS_2 and MoS_2 . Our results set the stage for further study on the electric field tunable 2D TMDCs devices.

See the [supplementary material](#) for the Materials and methods, PL spectrum of 2D TMDCs sandwiched by hBN and on a SiO_2 substrate, different bilayer devices, a clarification of the charge doping effect and the electric field effect with dual gate geometry, the displacement field dependence of PL intensity in monolayer WSe_2 , PL spectrum of bilayer WSe_2 measured at $D = 0$ V/nm and -1.5 V/nm, PL spectrum of bilayer WSe_2 under various displacement fields and DFT calculated band structure evolution of bilayer WSe_2 under various displacement fields.

G.Z. thanks the National Science Foundation of China (NSFC) under Grant No. 11834017, the Strategic Priority Research Program of the Chinese Academy of Sciences (CAS) under Grant No.

XDB30000000, the Key Research Program of Frontier Sciences of the CAS under Grant No. QYZDB-SSW-SLH004, and the National Key R&D program under Grant No. 2016YFA0300904.

The authors declare that they have no competing interest.

REFERENCES

- ¹G.-B. Liu, D. Xiao, Y. Yao, X. Xu, and W. Yao, *Chem. Soc. Rev.* **44**, 2643 (2015).
- ²Q. H. Wang, K. Kalantar-Zadeh, A. Kis, J. N. Coleman, and M. S. Strano, *Nat. Nanotechnol.* **7**, 699 (2012).
- ³B. Radisavljevic, A. Radenovic, J. Brivio, V. Giacometti, and A. Kis, *Nat. Nanotechnol.* **6**, 147 (2011).
- ⁴D. Xiao, G.-B. Liu, W. Feng, X. Xu, and W. Yao, *Phys. Rev. Lett.* **108**, 196802 (2012).
- ⁵T. Cao, G. Wang, W. Han, H. Ye, C. Zhu, J. Shi, Q. Niu, P. Tan, E. Wang, B. Liu, and J. Feng, *Nat. Commun.* **3**, 887 (2012).
- ⁶K. F. Mak, K. L. McGill, J. Park, and P. L. McEuen, *Science* **344**, 1489 (2014).
- ⁷G. Aivazian, Z. Gong, A. M. Jones, R.-L. Chu, J. Yan, D. G. Mandrus, C. Zhang, D. Cobden, W. Yao, and X. Xu, *Nat. Phys.* **11**, 148 (2015).
- ⁸A. M. Jones, H. Yu, J. S. Ross, P. Klement, N. J. Ghimire, J. Yan, D. G. Mandrus, W. Yao, and X. Xu, *Nat. Phys.* **10**, 130 (2014).
- ⁹P. Rivera, K. L. Seyler, H. Yu, J. R. Schaibley, J. Yan, D. G. Mandrus, W. Yao, and X. Xu, *Science* **351**, 688 (2016).
- ¹⁰P. Rivera, J. R. Schaibley, A. M. Jones, J. S. Ross, S. Wu, G. Aivazian, P. Klement, K. Seyler, G. Clark, N. J. Ghimire, J. Yan, D. G. Mandrus, W. Yao, and X. Xu, *Nat. Commun.* **6**, 6242 (2015).
- ¹¹B. Zhu, H. Zeng, J. Dai, Z. Gong, and X. Cui, *Proc. Natl. Acad. Sci. U. S. A.* **111**, 11606 (2014).
- ¹²K. Kang, S. Xie, L. Huang, Y. Han, P. Y. Huang, K. F. Mak, C.-J. Kim, D. Muller, and J. Park, *Nature* **520**, 656 (2015).
- ¹³Z. Zhang, P. Chen, X. Duan, K. Zang, J. Luo, and X. Duan, *Science* **357**, 788 (2017).
- ¹⁴S. Xie, L. Tu, Y. Han, L. Huang, K. Kang, K. U. Lao, P. Poddar, C. Park, D. A. Muller, and R. A. DiStasio, *Science* **359**, 1131 (2018).
- ¹⁵P. K. Sahoo, S. Memaran, Y. Xin, L. Balicas, and H. R. Gutiérrez, *Nature* **553**, 63 (2018).
- ¹⁶P. Chen, Z. Zhang, X. Duan, and X. Duan, *Chem. Soc. Rev.* **47**, 3129 (2018).
- ¹⁷A. Ramasubramaniam, D. Naveh, and E. Towe, *Phys. Rev. B* **84**, 205325 (2011).
- ¹⁸X. Dai, W. Li, T. Wang, X. Wang, and C. Zhai, *J. Appl. Phys.* **117**, 084310 (2015).
- ¹⁹K. H. Khoo, M. S. C. Mazzoni, and S. G. Louie, *Phys. Rev. B* **69**, 201401 (2004).
- ²⁰T. Chu, H. Ilatikhameh, G. Klimeck, R. Rahman, and Z. Chen, *Nano Lett.* **15**, 8000 (2015).
- ²¹J. Klein, J. Wierzbowski, A. Regler, J. Becker, F. Heimbach, K. Müller, M. Kaniber, and J. J. Finley, *Nano Lett.* **16**, 1554 (2016).
- ²²Z. Wang, Y.-H. Chiu, K. Honz, K. F. Mak, and J. Shan, *Nano Lett.* **18**, 137 (2018).
- ²³K. Watanabe, T. Taniguchi, and H. Kanda, *Nat. Mater.* **3**, 404 (2004).
- ²⁴Q. Ma, T. I. Andersen, N. L. Nair, N. M. Gabor, M. Massicotte, C. H. Lui, A. F. Young, W. Fang, K. Watanabe, T. Taniguchi, J. Kong, N. Gedik, F. H. L. Koppens, and P. Jarillo-Herrero, *Nat. Phys.* **12**, 455 (2016).
- ²⁵A. A. Obafunso, J. V. Ardelean, G. D. Shepard, J. Wang, A. Abhinandan, T. Taniguchi, K. Watanabe, T. F. Heinz, S. Strauf, X. Y. Zhu, and J. C. Hone, *2D Mater.* **4**, 031011 (2017).
- ²⁶C. R. Dean, A. F. Young, I. Meric, C. Lee, L. Wang, S. Sorgenfrei, K. Watanabe, T. Taniguchi, P. Kim, K. L. Shepard, and J. Hone, *Nat. Nanotechnol.* **5**, 722 (2010).
- ²⁷X. Cui, G.-H. Lee, Y. D. Kim, G. Arefe, P. Y. Huang, C.-H. Lee, D. A. Chenet, X. Zhang, L. Wang, F. Ye, F. Pizzocchero, B. S. Jessen, K. Watanabe, T. Taniguchi, D. A. Muller, T. Low, P. Kim, and J. Hone, *Nat. Nanotechnol.* **10**, 534 (2015).
- ²⁸L. Li, F. Yang, G. J. Ye, Z. Zhang, Z. Zhu, W. Lou, X. Zhou, L. Li, K. Watanabe, T. Taniguchi, K. Chang, Y. Wang, X. H. Chen, and Y. Zhang, *Nat. Nanotechnol.* **11**, 593 (2016).
- ²⁹Y. Hoshi, T. Kuroda, M. Okada, R. Moriya, S. Masubuchi, K. Watanabe, T. Taniguchi, R. Kitaura, and T. Machida, *Phys. Rev. B* **95**, 241403 (2017).
- ³⁰J. Wierzbowski, J. Klein, F. Sigger, C. Straubinger, M. Kremser, T. Taniguchi, K. Watanabe, U. Wurstbauer, A. W. Holleitner, M. Kaniber, K. Müller, and J. J. Finley, *Sci. Rep.* **7**, 12383 (2017).
- ³¹S. Jiang, L. Li, Z. Wang, K. Mak, and J. Shan, *Nat. Nanotechnol.* **13**, 549 (2018).
- ³²L. Fumagalli, A. Esfandiari, R. Fabregas, S. Hu, P. Ares, A. Janardanan, Q. Yang, B. Radha, T. Taniguchi, K. Watanabe, G. Gomila, K. S. Novoselov, and A. K. Geim, *Science* **360**, 1339 (2018).
- ³³W. Zhao, R. M. Ribeiro, M. Toh, A. Carvalho, C. Kloc, A. H. Castro Neto, and G. Eda, *Nano Lett.* **13**, 5627 (2013).
- ³⁴C. Zhang, Y. Chen, A. Johnson, M.-Y. Li, L.-J. Li, P. C. Mende, R. M. Feenstra, and C.-K. Shih, *Nano Lett.* **15**, 6494 (2015).
- ³⁵H. Yuan, Z. Liu, G. Xu, B. Zhou, S. Wu, D. Dumcenco, K. Yan, Y. Zhang, S.-K. Mo, P. Dudin, V. Kandyba, M. Yablonskikh, A. Barinov, Z. Shen, S. Zhang, Y. Huang, X. Xu, Z. Hussain, H. Y. Hwang, Y. Cui, and Y. Chen, *Nano Lett.* **16**, 4738 (2016).
- ³⁶L. Du, T. Zhang, M. Liao, G. Liu, S. Wang, R. He, Z. Ye, H. Yu, R. Yang, D. Shi, Y. Yao, and G. Zhang, *Phys. Rev. B* **97**, 165410 (2018).
- ³⁷J. He, K. Hummer, and C. Franchini, *Phys. Rev. B* **89**, 075409 (2014).
- ³⁸K. F. Mak, K. He, C. Lee, G. H. Lee, J. Hone, T. F. Heinz, and J. Shan, *Nat. Mater.* **12**, 207 (2013).
- ³⁹F. Withers, O. Del Pozo-Zamudio, A. Mishchenko, A. P. Rooney, A. Gholinia, K. Watanabe, T. Taniguchi, S. J. Haigh, A. K. Geim, A. I. Tartakovskii, and K. S. Novoselov, *Nat. Mater.* **14**, 301 (2015).
- ⁴⁰X. Zhang, Y. You, S. Yang, F. Zhao, and T. F. Heinz, *Phys. Rev. Lett.* **115**, 257403 (2015).